Research Article | Open Access

Microstructures

Qian *et al*. *Microstructures* **2026**, *6*, 2026067 **DOI:**10.20517/microstructures.2025.134

Microstructure engineering of core-shell flame retardants: SiO_2 and MXene encapsulated ammonium polyphosphate for fire-safe thermoplastic polyurethane

Xiaodong Qian[1,#], Mei Wan[1,#], Yanan Hou[1,2], Congling Shi[1], Lei Chen[1], Honglei Che[1], Jingyun Jing[1], Jian Li[1], Ye-Tang Pan[1,3]

Keywords:
Microstructure design, flame retardancy, core-shell structure, MXene, ammonium polyphosphate, thermoplastic polyurethane

Citation: Qian, X.; Wan, M.; Hou, Y.; Shi, C.; Chen, L.; Che, H.; Jing, J.; Li, J.; Pan, Y. T. Microstructure engineering of core-shell flame retardants: SiO_2 and MXene encapsulated ammonium polyphosphate for fire-safe thermoplastic polyurethane. *Microstructures* **2026**, *6*, 2026067. https://dx.doi.org/10.20517/microstructures.2025.134

Received: 26 Sep 2025 **First Decision:** 19 Dec 2025 **Revised:** 4 Jan 2026 **Accepted:** 23 Jan 2026 **Published:** 18 May 2026

Academic Editor: Zhanxi Fan
Copy Editor: Ping Zhang
Production Editor: Ping Zhang

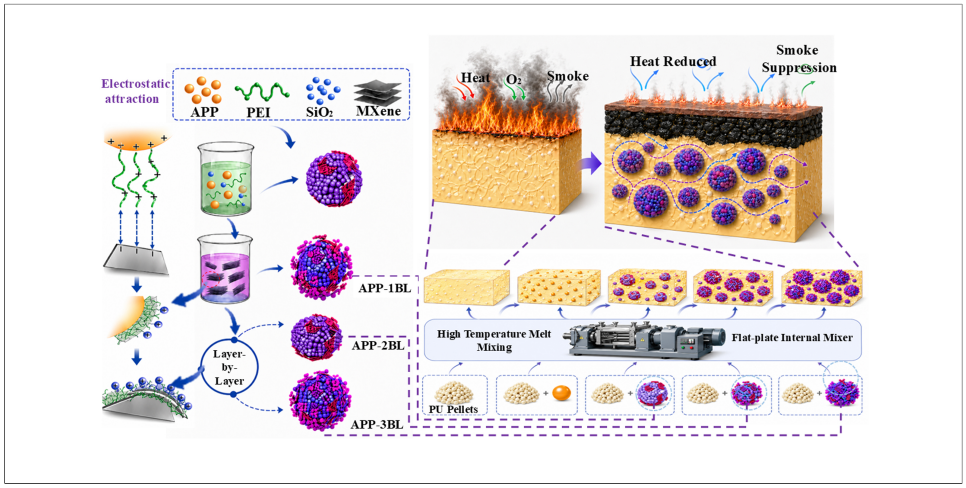

Abstract

Microstructure manipulation represents a fundamental strategy for enhancing material properties. Herein, a new-type flame-resistant material with core-shell architecture (APP@PEI@SiO_2@MXene) is prepared by iterative deposition of self-assembled monolayers, enabling microstructural control of ammonium polyphosphate (APP) via sequential coating with polyethyleneimine (PEI), SiO_2, and MXene. Then the flame retardants were incorporated into thermoplastic polyurethane (TPU) at a loading of 15 wt.%, this meticulously designed microstructure enables the composite to exhibit significantly improved fire safety. The composite exhibits a markedly increased high-temperature char residue under both air and nitrogen atmospheres, indicating improved thermal resilience and char formation capacity. Thermal stability analysis of the material reveals that the coated APP enables TPU composites to engender a carbonaceous stratum of heightened tenacity. Cone calorimetry tests indicate that, compared with pure TPU, TPU/APP-1BL composites exhibit sharp declines of 87.90% in total heat release

[1]Beijing Key Laboratory of Metro Fire and Passenger Transportation Safety, China Academy of Safety Science and Technology, Beijing 100012, China.
[2]College of Geological Engineering and Geomatics, Chang'an University, Xian 710018, Shaanxi, China.
[3]National Engineering Research Center of Flame Retardant Materials, School of Materials Science & Engineering, Beijing Institute of Technology, Beijing 100081, China.
[#]Authors contributed equally.

Correspondence to: Prof. Congling Shi, Beijing Key Laboratory of Metro Fire and Passenger Transportation Safety, China Academy of Safety Science and Technology, Beijing 100012, China. E-mail: shicl@chinasafety.ac.cn; Prof. Ye-Tang Pan, National Engineering Research Center of Flame Retardant Materials, School of Materials Science & Engineering, Beijing Institute of Technology, Beijing 100081, China. E-mail: pyt@bit.edu.cn

(THR) and 76.79% in the peak heat release rate (pHRR), with concurrent effective control of smoke/toxic gas emissions. Moreover, the flame-retardant effects of multi-layer coated APP are notably better than those of single-layer coated APP. Mechanistic studies reveal that the flame-retardant performance chiefly originates from the synergistic interplay of solid and vapor-stage pathways. This work highlights the critical role of microstructure design in the creation of high-performance fire-resistant polymers.

INTRODUCTION

Due to the widespread adoption and advancement of polymer materials, plastic products are widely used[1-3]. Among them, thermoplastic polyurethane (TPU) is extensively applied across varied sectors including military, aerospace, automotive, electronics, appliances, and biomedicine, owing to its advantages of oil resistance, low temperatures, aging, radiation, biocompatibility, and ease of processing[4-6]. Nevertheless, TPU materials exhibit combustibility and release substantial quantities of toxic fumes and particulate matter when burned, causing enduring environmental harm, loss of life, and economic losses, thereby limiting its utility across various sectors[7-9]. Thus, enhancing the fire-resistance performance of TPU is highly imperative.

It is well known that the combustion of TPU materials typically begins with thermal degradation when exposed to external thermal sources. With rising temperature, thermal influence induces progressive degradation of hydrogen-bonded physical cross-links within TPU's hard segments. Macromolecular chain interactions diminish and ultimately rupture, generating volatile fragments. In addition, the TPU, as the combustible material, generates thermal radiation that feeds back into the combustion area, providing a continuous source of energy for the combustion reaction, thereby creating a vicious cycle[10,11]. Nonetheless, incorporating flame retardants may disrupt polyurethane's combustion process by postponing polymer ignition timing, inhibiting the spread of the polymer flame, and minimizing the emission of heat as well as toxic and harmful gases from the polymer. Consequently, this diminishes the polymer's flammability hazard, necessitating high-efficiency flame retardant modification for TPU materials.

In recent years, ammonium polyphosphate (APP) is broadly utilized in flame-retardant applications due to its elevated phosphorus-nitrogen ratio and economical cost[12,13]. During gas-phase decomposition, APP releases abundant non-flammable ammonia, diluting ambient oxygen and thereby quenching continuous burning of the polymer matrix. In the condensed phase, a significant amount of polyphosphoric acid, as well as pyrophosphoric acid, is produced. These function as potent dehydrating agents, accelerating the carbonization and dehydration of the polymer chains, thereby generating a compact char barrier at the substrate surface that insulates heat and blocks oxygen. However, APP has disadvantages such as high water solubility, strong hygroscopicity, and poor compatibility with the matrix material, which limits its flame retardant efficiency[14-16]. APP's flame-retardant application remains severely constrained. To address the above issues, methods such as coupling agent modification, microencapsulation, and ultrafine processing are employed to improve the situation. Moreover, under specific conditions, supplementary nanoscale synergists remain indispensable for effectively augmenting APP's flame-retardant efficacy.

Among diverse surface engineering approaches for APP, microencapsulation has been validated as an efficient strategy to resolve challenges of suboptimal flame retardancy and inadequate dispersion[17,18]. However, when selecting the shell material for microencapsulation, factors such as cost and processability also need to be considered. In some cases, extra co-retardants are still needed to enhance the fire-retardant

efficacy of microencapsulated APP[19,20]. At the same time, it has not been found that anyone has used MXene and silica as raw materials for the microencapsulation of APP. Existing studies on the influence of modifier dosage in surface-modified APP on polymer flame retardancy and smoke suppression properties remain insufficiently comprehensive.

In contrast to alternative flame retardants, nanoscale systems exhibit a notably distinct characteristic, they exhibit extremely high efficiency in reducing the fire risk of polymers even when added at low concentrations (≤ 5%)[21-25]. Among various nanoscale flame retardants, MXene, a rapidly developing two-dimensional nanomaterial, is considered a promising nano-additive for wide-ranging flame retardant applications[26]. Chen electrostatically assembled Prussian-blue analogues(PBAs) on MXene sheets to build hierarchical MXene@PBA hybrids; adding only 1.0 wt.% to epoxy elevated the flame-retardancy classification of the ensuing material to the apex tier of the UL-94 protocol V-0[27]. A hierarchical MXene nanosheet sheathed with bimetallic phosphates (MXene@NCP) was synthesized by Zhou and colleagues through a solvothermal approach. When incorporated into an epoxy resin (EP) at a low loading of 2 wt.%, this filler remarkably suppressed the material's flammability, reducing the peak heat release rate and the peak CO generation rate by 35.5% and 34.8%, respectively[28]. Some studies have found that MXene, as a synergist, demonstrates improved flame-retardant performance when paired with other flame retardants[29,30]. However, the stacking issue of MXene in polymers needs to be addressed through functional modification of MXene[31,32].

Hence, by fully leveraging the properties of silica and MXene and adopting the sequential layer-by-layer assembly to modify APP, the core solution to address the low flame-retardant efficiency of APP (APP@PEI@SiO_2@MXene) is achieved, endowing APP with substantially upgraded fire-barrier and smoke-suppression capabilities. The TPU material's high-temperature thermal stability was notably improved, and it's also found that the barrier effects of layered MXene, dense SiO_2 oxide film, phosphorus-rich glassy substances, and expanded carbon layers served as a pivotal factor in elevating fire-retardant effectiveness. This work highlights the critical role of microstructure design in the creation of high-performance fire-resistant polymers.

MATERIALS AND METHODS

Materials

4190-grade TPU was supplied by Foshan Pinchen Trading Co., Ltd., Guangdong, China. Titanium Aluminum Carbide (MAX) was provided by Laizhou Kai Kai Ceramic Materials Co., Ltd., Shandong, China. Hydrochloric acid (HCl, AR), ethanol (AR), and tetraethyl orthosilicate (TEOS, AR) were acquired from Sinopharm Chemical Reagent Co., Ltd., Shanghai, China. Ammonium polyphosphate (APP, ≥ 1,000 grade) was obtained from Macklin Biochemical Co., Ltd., Shanghai, China. Polyethyleneimine (PEI, Mw 70000, 50% aqueous) and lithium fluoride (LiF) were purchased from Shanghai Aladdin Bio-Chem Technology Co., Ltd., Shanghai, China.

Preparation of MXene and APP@PEI@SiO_2@MXene

The preparation method of MXene was referred to previous reports[33,34]. A quantity of 3 grams of PEI was introduced into the mixtures of 800 mL water-ethanol (1:1) and agitated for a duration of 30 min under ambient temperature. Subsequently, following the dropwise addition of 6 mL of TEOS to the mixed solution, the reaction was maintained at 80 °C for 3 h, ultimately yielding a milky white suspension. Finally, the white PEI@SiO_2 powders were collected after centrifugal separation, rinsing, and drying.

The synthetic pathway of modified APP are shown in Figure 1. 10 g of APP was dissolve in 200 mL deionized water, and added into 100 mL of PEI@SiO_2 solution (6 mg/mL), and the precipitate was wash by water and centrifuge (room temperature, 6,000 rpm) 3 times. Then, the above precipitate was again dissolved

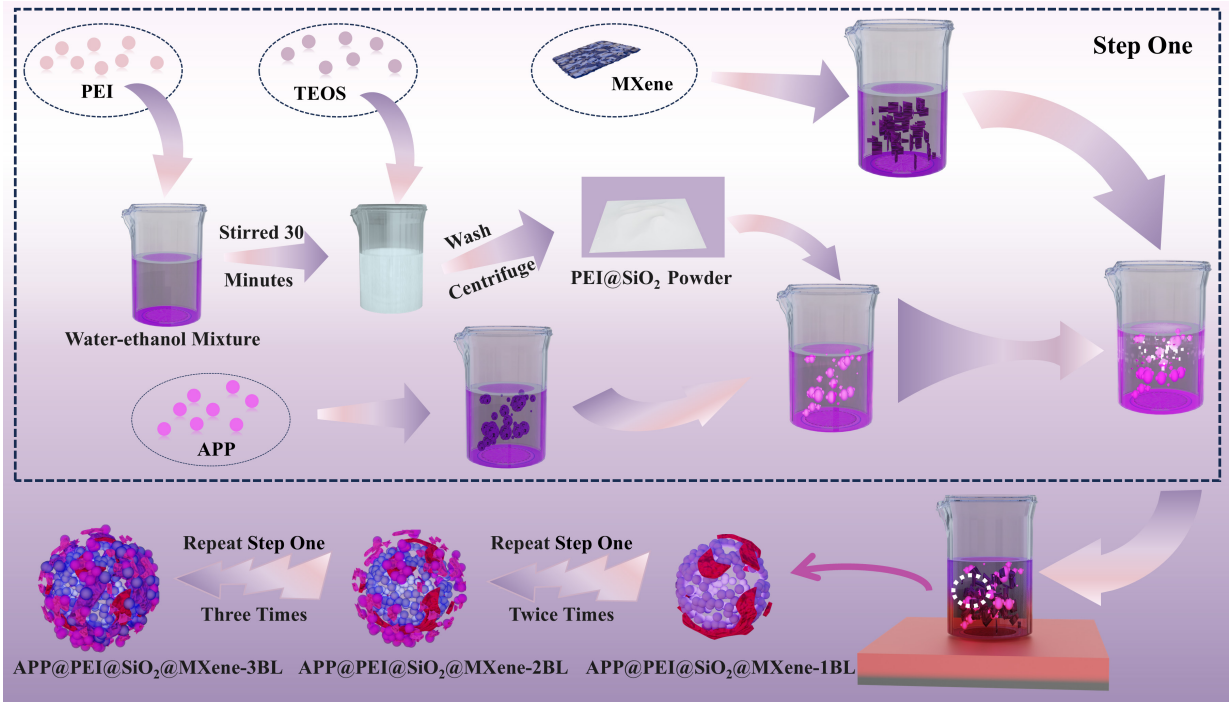

Figure 1. Schematic diagram for the synthetic pathway of APP-1BL. PEI: Polyethyleneimine; TEOS: tetraethyl orthosilicate; APP: ammonium polyphosphate.

Table 1. Thermal degradation profiles of the investigated composites under controlled atmospheres: (a, b) N_2 and (c, d) air

Sample	Composite formulations	Nitrogen				Air				
		T_i (°C)	T_{max} (°C)		$R_{600°C}$ (wt.%)	T_i (°C)	T_{max} (°C)			$R_{900°C}$ (wt.%)
			T_{1max}	T_{2max}			T_{1max}	T_{2max}	T_{3max}	
TPU-0	TPU 100wt.%	315.09	332.50	396.16	7.34 ± 0.13	303.37	327.00	385.67	564.93	0.76 ± 0.02
TPU-1	TPU 85wt.%; APP 15wt.%	268.60	277.71	316.27	28.89 ± 0.14	267.63	278.85	328.46	535.93	6.05 ± 0.12
TPU-2	TPU 85wt.%; APP-1BL 15wt.%	262.04	274.27	320.39	32.10 ± 0.15	265.11	277.75	334.07	548.33	6.67 ± 0.13
TPU-3	TPU 85wt.%; APP-2BL 15wt.%	261.63	275.06	317.23	32.44 ± 0.21	262.45	276.59	330.19	550.31	6.40 ± 0.13
TPU-4	TPU 85wt.%; APP-3BL 15wt.%	265.78	276.17	312.12	30.82 ± 0.22	264.66	277.22	325.47	523.03	6.83 ± 0.11

TPU: Thermoplastic polyurethane; APP: ammonium polyphosphate.

in 200 mL ion-free water, then added into 100 mL MXene solution (1 mg/mL), and the precipitate was wash and centrifuge (room temperature, 6,000 rpm) for 3 times, and then APP@PEI@SiO_2@MXene-1BL (APP-1BL) was obtained. The above-listed steps were repeated 3 times, yielding the products APP@PEI@SiO_2@MXene-2BL (APP-2BL) and APP@PEI@SiO_2@MXene-3BL(APP-3BL).

Preparation of TPU composites

A mixtures of 42.5 g of TPU and 7.5 g of APP were blended confidentially at a temperature of 185 °C, utilizing a flat vulcanization press plate TPU containing 15 wt.% APP at a range of 185-190 °C. Pure TPU and its flame-retardant counterparts containing APP@PEI@SiO_2@MXene were fabricated through an identical protocol, the composition and codes of the composite materials are listed in Table 1.

Characterization and analytical evaluation

The structural and chemical attributes of the char layers were interrogated using a suite of characterization techniques: scanning electron microscopy (SEM, Phenom XL G2, Netherlands) for microstructural

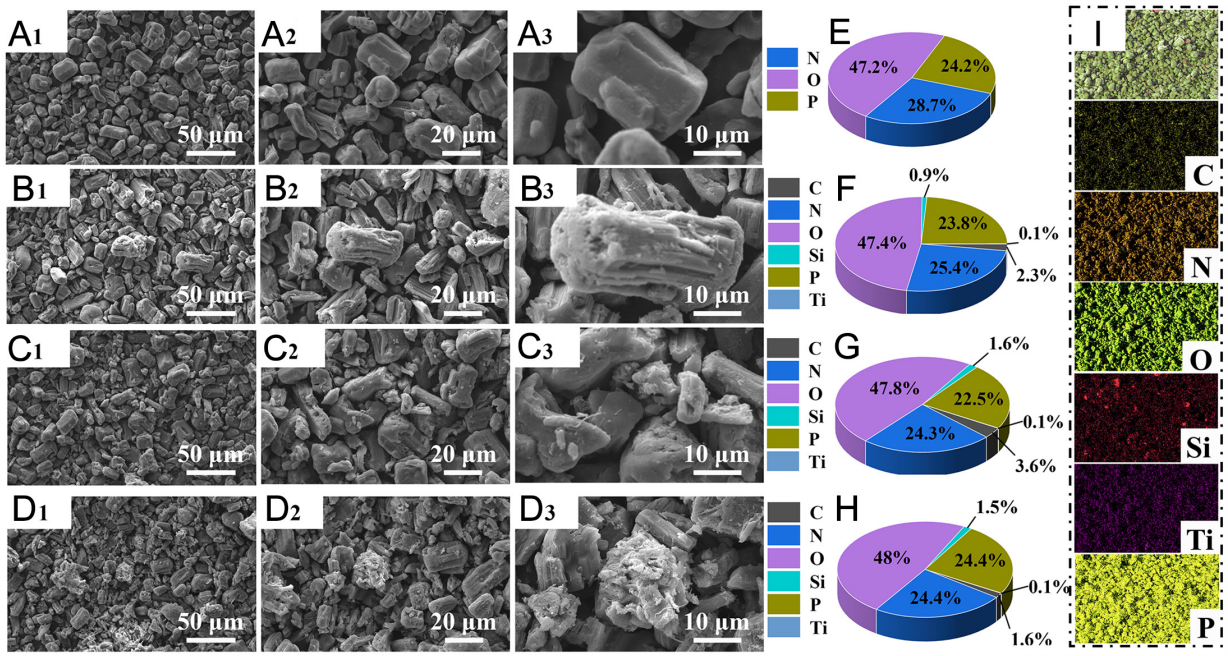

Figure 2. Field-emission scanning electron micrographs and energy-dispersive X-ray spectra for (A_1, A_2, A_3 and E) neat APP, (B_1, B_2, B_3 and F) APP-1BL, (C_1, C_2, C_3 and G) APP-2BL, (D_1, D_2, D_3 and H) APP-3BL; elemental cartography micrograph of (I) APP-3BL. APP: Ammonium polyphosphate.

morphology; X-ray photoelectron spectroscopy (XPS, Thermo ESCALAB 250 Xi, USA) for elucidating elemental chemical states, complemented by energy-dispersive X-ray spectroscopy (EDS, same platform) for elemental mapping; X-ray diffraction (XRD, Bruker) for crystalline phase identification; and Fourier-transform infrared spectroscopy (FTIR, NICOLET IS10, USA) for functional group determination. A Raman spectrometer (Renishaw inVia, UK) further characterized the carbonaceous residue. Thermogravimetric analysis (TGA 550) was conducted under nitrogen or air to evaluate thermal stability. The cone calorimeter test (CCT, FTT, UK) at 35 kW m^{-2} supplied the combustion parameters, and each sample was tested three times using the cone calorimeter, and the average value of the three replicate tests was adopted.

RESULTS AND DISCUSSION

Characterization of APP@PEI@SiO_2@MXene

The SEM images of flame retardants before and after modification via self-assembly are shown in Figure 2. For pristine APP, its surface is remarkably smooth; however, after undergoing self-assembly and being coated with SiO_2 and MXene, as shown in Figure 2B, its surface morphology transforms into a rough state featuring numerous small particles evenly adsorbed onto the APP surface - this is largely attributed to SiO_2 and MXene. Moreover, a progressive increase in the number of self-assembly layers leads to a rougher APP surface. According to the EDS maps in Figure 2E, F and H, surface Si in the encapsulated APP accumulates progressively as the coating cycles increase, while the P content steadily decreases; yet for APP-3BL, the P content actually increases-this implies that a 2-layer coating is a critical layer count for APP modification, and further increasing the number of modified layers beyond this point is actually detrimental to the coverage of SiO_2 and MXene. Meanwhile, the elemental distribution of APP-3BL verifies that the shell materials SiO_2 and MXene are uniformly dispersed on the surface of the APP combustion inhibitor, which can efficaciously improve the surface interfacial performance of APP. As illustrated in Figure 3A, Elemental compositions of APP and modified APP were mapped by EDS. It is observed that the main elements in modified APP include N, O, P, Si, and Ti, whereas Si and Ti are not present in APP-this confirms the multiple coatings of PEI@SiO_2@MXene on the APP surface.

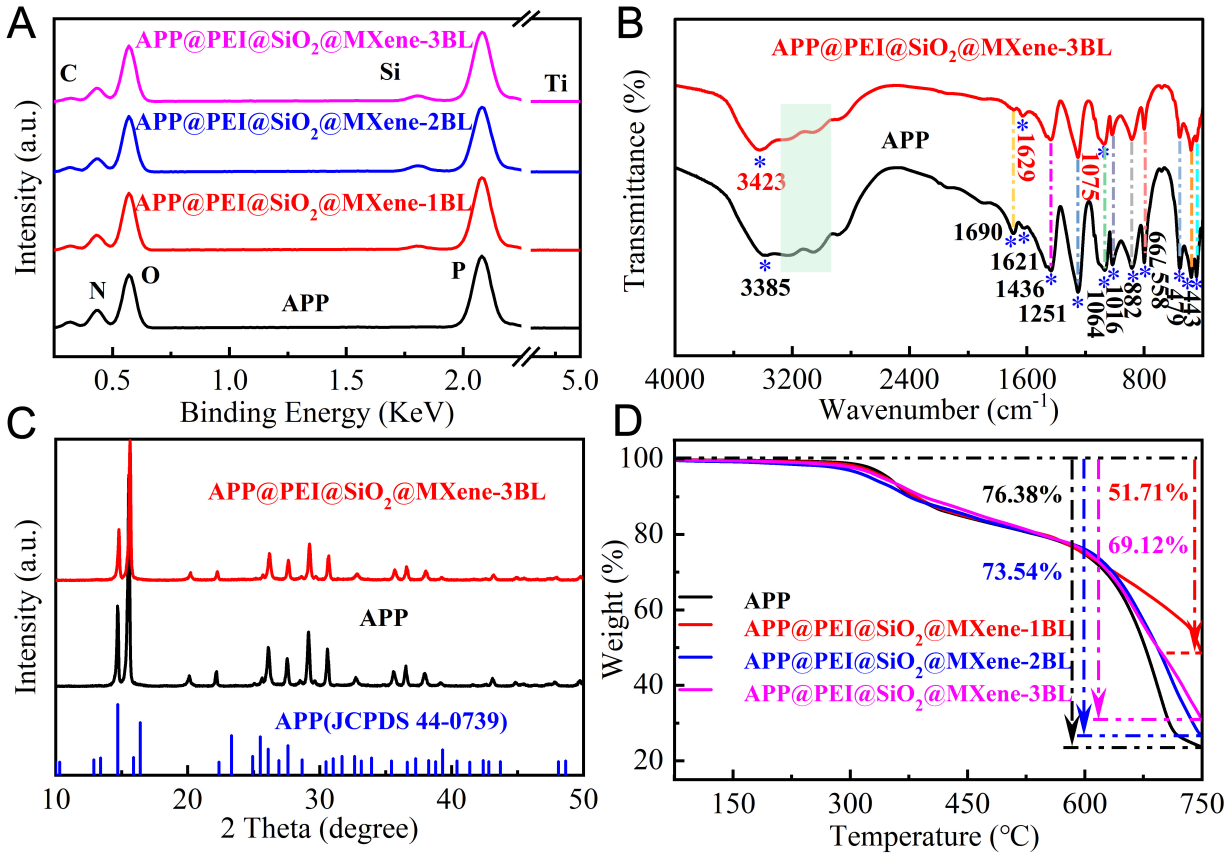

Figure 3. (A) EDS; (B) FTIR; (C) XRD; (D) TGA of APP and APP@PEI@SiO_2@MXene. EDS: Energy-dispersive X-ray spectroscopy; FTIR: Fourier-transform infrared spectroscopy; XRD: X-ray diffraction; TGA: thermogravimetric analysis; APP: ammonium polyphosphate; PEI: polyethyleneimine.

As illustrated in Figure 3B, Fourier-transform infrared spectroscopy was utilized to probe the molecular functionalities of APP and its modified counterpart, APP-3BL. The APP spectrum manifested distinctive absorption bands centered at 3,385 and 3,209 cm^{-1}, attributable to hydroxyl (-OH) and amino (N-H) moieties, respectively. Further diagnostic signals emerged at 1,251 cm^{-1} (P-O bonding), 1,064 cm^{-1} (symmetric P-O elongation), 1,016 cm^{-1} (symmetric PO_2 and PO_3 vibrations), and 882 cm^{-1} (asymmetric P-O elongation concurrent with P-O-P linkage). Upon the successive deposition of SiO_2 and MXene layers to yield APP-3BL, a new, well-defined band materialized at 3,423 cm^{-1}, indicative of O-H valence vibration. The spectral signature of MXene became particularly pronounced within the 1,000-1,800 cm^{-1} window. A definitive band near 550 cm^{-1} corroborates the existence of Ti-O bonding. Additionally, spectral contributions from C-O and C=O groups were discerned within the 1,500-1,700 cm^{-1} interval[35-37]. The spectral profile of APP-3BL also featured a band at 443 cm^{-1}, ascribed to the Si-O motional mode. Concurrently, additional spectral features at 1,018, 780, and 479 cm^{-1} signify the emergence of hybridization effects.

Further studies on the crystalline structure of APP and modified APP were conducted by XRD in Figure 3C. All APP reflections align with those of standard JCPDS 44-0739, confirming phase purity. For MXene, its 18.6° (004), 25.5° (006), 34.1° (011) and 38.9° (014) reflections coincide with those of APP in APP-3BL, evidencing that PEI@SiO_2@MXene is present as an ultrathin sheath enveloping the APP core[38,39]. Figure 3D presents the thermogravimetric results, which indicate that by virtue of the synergistic interaction between PEI@SiO_2@MXene and APP, the high-temperature carbonization performance of modified APP is substantially improved-this in turn enhances its flame-retardant performance.

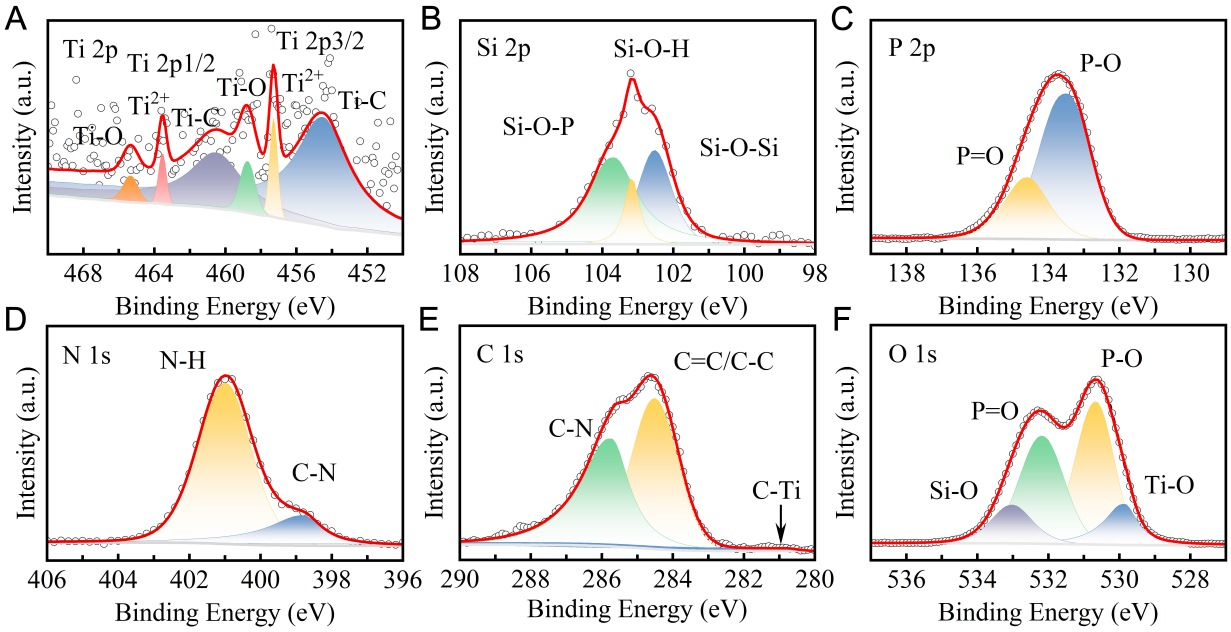

Figure 4. High-resolution (A) Ti 2p, (B) Si 2p, (C) P 2p, (D) N 1s, (E) C 1s, and (F) O 1s XPS spectra for APP-3BL. APP: Ammonium polyphosphate; XPS: X-ray photoelectron spectroscopy.

To further resolve the surface-element distribution of the flame retardant, the APP-3BL sample was surveyed by XPS; the spectra are displayed in Figure 4. As for APP-3BL, the characteristic peaks of Si and Ti appeared near 102 and 455 eV, respectively. The Si absorption peaks mainly included Si-OH, Si-O-Si, and Si-O-P structures, demonstrating that a chemical reaction took place between nano-silica and APP during the self-assembly process, leading to the formation of Si-O-P structures. Furthermore, the Ti 2p signals further verify that MXene is anchored on the APP surface[40,41]. XPS data indicate that the surface element content of the flame retardant has changed after microencapsulation, with a significant presence of characteristic modified elements Si and Ti.

Thermal stability of the composites

Figure 5 illustrates the TGA profiles of the composites measured in nitrogen and air atmospheres. Under N_2, the TPU composite degrades in two well-resolved steps: hard-segment scission first, followed by soft-segment depolymerisation[42,43]. Pure TPU demonstrates relatively high thermal stability below 330 °C. Additionally, the TGA curve reveals a slight decline in stability above 400 °C, and elevated temperatures further accelerate its thermal degradation rate. Pure TPU exhibits a relatively high initial decomposition temperature (T_i), with its maximum decomposition rate peaking at 396.16 °C. This behavior indicates that while the hard segments of TPU decompose with considerable stability, the soft segments undergo accelerated decomposition due to uncontrolled breakdown. Pure TPU leaves a relatively low char residue of merely 7.34 wt.% (see Table 1). Generally, APP usually decomposes to generate strong phosphorus-containing acids, such as phosphoric acid, pyrophosphoric acid, and metaphosphoric acid, and these acids display catalytic activity in breaking polyurethane bonds into compounds such as alcohols, isocyanates, and CO_2, which leads to the early degradation observed in TPU/APP blends and their flame-retardant composites. The composite material undergoes thermal degradation at a lower temperature, which indicates that SiO_2 and MXene can slightly facilitate the thermal degradation of the composite, form a stable carbon layer ahead of time, and exert a flame-retardant effect at low temperatures. Furthermore, the residual char contents of TPU/APP and TPU/APP@PEI@SiO_2@MXene composites at 600 °C are 28.89 wt.% and 32.44 wt.%, respectively. The high char residues at elevated temperatures suggest a synergistic effect between APP and PEI@SiO_2@MXene:

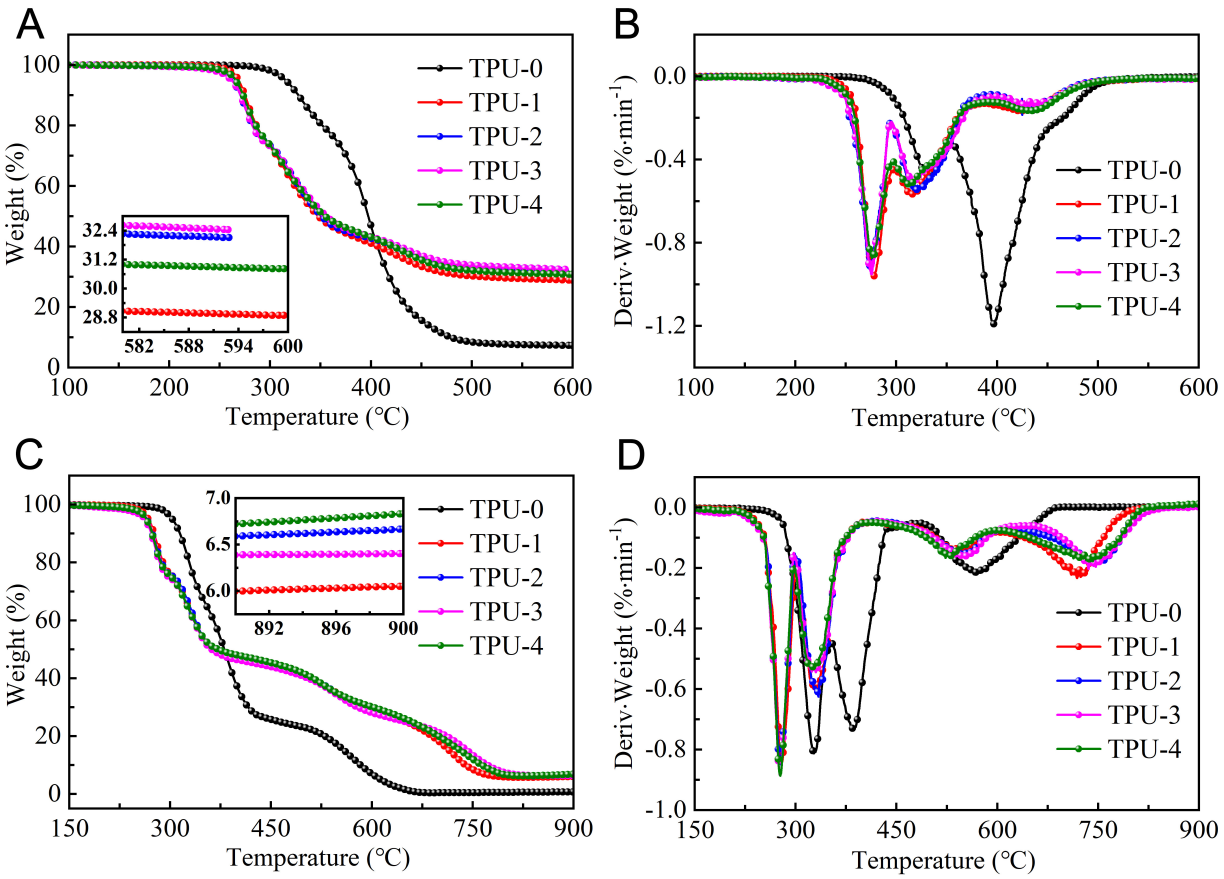

Figure 5. Thermogravimetric Analysis and corresponding derivative profiles of the composite materials under inert (A and B) and oxidative (C and D) conditions. TPU: Thermoplastic polyurethane.

As depicted in Figures 5C and D, under an air atmosphere, the oxidative decomposition of TPU composites comprises three stages. The breakdown of polyurethane bonds serves as the main process in the initial stage; conversely, the second and third stages primarily involve polyol decomposition. The distribution patterns of T_i and T_{max} are mostly in line with those in an N_2 atmosphere, while the distribution pattern of residual carbon varies from that in a nitrogen atmosphere. Furthermore, a notable increase in char residue is observed for the TPU/APP@PEI@SiO_2@MXene composite at 350 °C compared to the TPU/APP composite, and the composite containing APP-3BL possesses the highest residual carbon content. Because a high residual carbon content benefits the improvement of flame retardant performance, APP-3BL is the most effective in boosting the composites' flame retardancy. Meanwhile, the measurement outcomes of TGA residual carbon are mostly in agreement with the CCT results.

Combustion behavior of the composites

The Cone Calorimeter is regarded as the most effective technical method for measuring the combustion characteristics of materials, as its combustion environment closely resembles actual combustion conditions compared to other technical methods. Cone calorimetry was used to quantify key fire-risk metrics - heat release, smoke evolution and mass loss - of the materials. The characteristic curves and key data of the combustion process for the composites are shown in Table 2 and Figure 6.

The results show pure TPU material is ignited within 55 s, while the initial ignition time for other composites is shorter than 50 s. This indicates that these two substances-APP and APP@PEI@SiO_2@MXene-demonstrate a catalytic function in the early decomposition of TPU. Pure TPU exhibits the highest values for peak heat

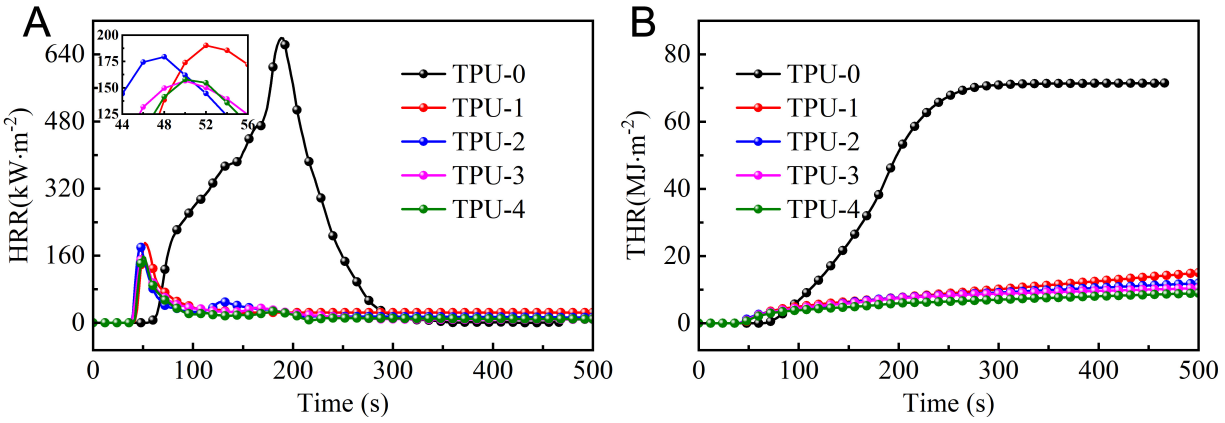

Figure 6. Combustion performance evaluation: (A) HRR and (B) THR of neat TPU versus its composite formulations. HRR: Heat release rate; THR: total heat release; TPU: thermoplastic polyurethane.

release rate (pHRR) and total heat release (THR), which are 678.56 kW/m² and 71.746 MJ/m², indicating the high fire risk. Relative to pure TPU material, the pHRR of TPU/APP composite drops to 190.27 kW/m² (a 71.96% reduction), while that of TPU/APP@PEI@SiO_2@MXene composite falls to 157.50 kW/m² (a 76.79% reduction). Furthermore, relative to neat TPU, the total heat release was curtailed by 79.0% with APP and by 87.90% upon incorporation of APP@PEI@SiO_2@MXene. And as the number of PEI@SiO_2@MXene coatings on the APP surface increases, the reduction effect of THR and pHRR of the composites becomes more significant, with TPU-3 and TPU-4 having the lowest pHRR and THR values respectively. To some extent, this reflects the synergistic flame retardancy between APP and PEI@SiO_2@MXene. This synergistic flame-retardant effect accelerates carbon formation, driving a marked reduction in heat release.

In a fire, smoke is a major cause of injuries and fatalities, with its release presenting greater peril than heat release. Data presented in Table 2 and Figure 7 indicate that pure TPU material has remarkably high values of Smoke Production Rate (SPR) (14.37 m²/s²), Total Smoke Production (TSP) (18.06 m²/m²), Yield of Carbon Monoxide (YCO) (0.0211 g/s), and Yield of Carbon Dioxide (YCO_2) (0.5950 g/s). The risk of using it directly without incorporating a smoke suppressant is incalculable, because the smoke released during the fire is often a significant factor in causing fatalities. Relative to neat TPU, the flame-retardant formulations exhibit an SPR drop of approximately 65.2%. In addition, the release of TSP, CO, and CO_2 for TPU/APP@PEI@SiO_2@MXene is significantly reduced, with the final TSP, YCO, and YCO_2 values decreasing to 1.64 m²/m², 0.0110 g/s, and 0.1080 g/s, respectively. With increasing PEI@SiO_2@MXene layers increases, the smoke suppression effect gradually enhances. These results indicate that the combination of PEI@SiO_2@MXene shell and APP at the micrometer scale has a significant smoke suppression effect. This may be due to the flame retardant APP@PEI@SiO_2@MXene enhancing the carbon strength of the polymer, thus effectively preventing the emission of toxic and harmful gases.

Figure 8 displays the specimen's mass-loss curve recorded in the cone test, which diverges from the TGA profiles obtained in both air and nitrogen. With a mere 7.73% residual mass, pure TPU shows high combustibility. This is countered by flame retardants, as the TPU composites then show reduced mass loss in a declining trend. Among these composites, the final char yield of the TPU/APP@PEI@SiO_2@MXene composite after 500 seconds of burning reaches up to 79.03%, which is totally distinct from the TGA pyrolysis outcomes of the material in air. The discrepancy in char residue rate between the cone calorimeter and TGA stems from differences in test environments and reaction mechanisms: the former simulates real combustion, while the latter is static pyrolysis. This discrepancy significantly reflects the intumescence (formation of a continuous and dense char layer) and drip suppression (reduction of mass loss) of the

Table 2. CCT parameters for TPU and its composite formulations

Sample	pHRR (kW/m²)	T_{pHRR} (s)	THR (MJ/m²)	FPI [m²/(s·kW)]	FSI [kW/(m²·s)]	SPR (m²/s²)	TSP (m²/m²)	Y_{CO} (g/s)	Y_{CO2} (g/s)	MASS (%)
TPU-0	678.56 ± 8.12	188.09	71.46 ± 3.78	0.08	3.61	14.37	18.06	0.0211	0.5950	7.73
TPU-1	190.27 ± 5.23	52.00	15.00 ± 1.34	0.20	3.66	5.01	3.73	0.0128	0.1326	72.74
TPU-2	181.10 ± 3.14	47.98	11.88 ± 0.78	0.19	3.77	4.60	2.11	0.0120	0.1231	77.07
TPU-3	157.50 ± 4.18	49.99	10.42 ± 0.68	0.23	3.15	5.30	1.78	0.0116	0.1036	78.29
TPU-4	159.00 ± 5.45	49.98	8.93 ± 0.74	0.25	3.18	4.65	1.64	0.0110	0.1080	79.03

TPU: Thermoplastic polyurethane; APP: ammonium polyphosphate; CCT: cone calorimeter test; pHRR: peak heat release rate; THR: total heat release; FSI: flame spread index; SPR: smoke production rate; TSP: total smoke production; MASS: mass loss rate; FPI: fire performance index.

material during combustion, rather than test condition artifacts. The discrepancy verifies the synergistic flame-retardant mechanism of the composite material and demonstrates better char layer retention capacity in real fire scenarios.

In summary, APP and modified APP can accelerate the degradation of TPU composites at low temperatures, rapidly forming stable char layers. Combined with monitoring results such as pHRR, THR, SPR, TSP, Y_{CO}, and Y_{CO2}, the integrity-preserving carbon layer can effectively isolate the transmission of heat and gas between the interior and exterior of the matrix. Thus, it enhances the flame retardant performance of TPU composites. Among them, TPU-4 exhibits the best overall flame retardant performance.

Morphological and structural characteristics of char residues

The structural morphology of the carbon layer is closely associated with the flame retardant ability of the composite. Hence, performing macroscopic structural morphology analysis on the residual carbon layer after cone calorimeter tests is a viable approach to elucidate its mode of flame retardant action. The composite's residual char is illustrated in Figure 9. For pure TPU, only a tiny quantity of carbon residue is left. After the combustion of untreated TPU composites, digital photos in Figure 9 demonstrate that pure TPU produces char residues with a relatively porous and fragmented morphology, featuring an incomplete thin carbon layer and insufficient expansion height. The enhanced flame retardancy is evidenced by the evolution of char morphology, as revealed by SEM. The char transitions from a cracked, porous structure in pure TPU to a continuous, dense, and expanded carbon barrier in the flame-retardant composites. Specifically, the TPU/APP@PEI@SiO_2@MXene composite forms a seamless and highly expanded char layer, a morphology that is markedly improved to the cracked carbon layer observed in TPU/APP composites. This morphological improvement directly contributes to fire suppression. Elemental mapping of the composite char further shows P, N, O, C, Si and Ti to be homogeneously spread throughout the layer, evidencing that well-distributed flame-retardant species actively promote the development of a continuous protective barrier during burning.

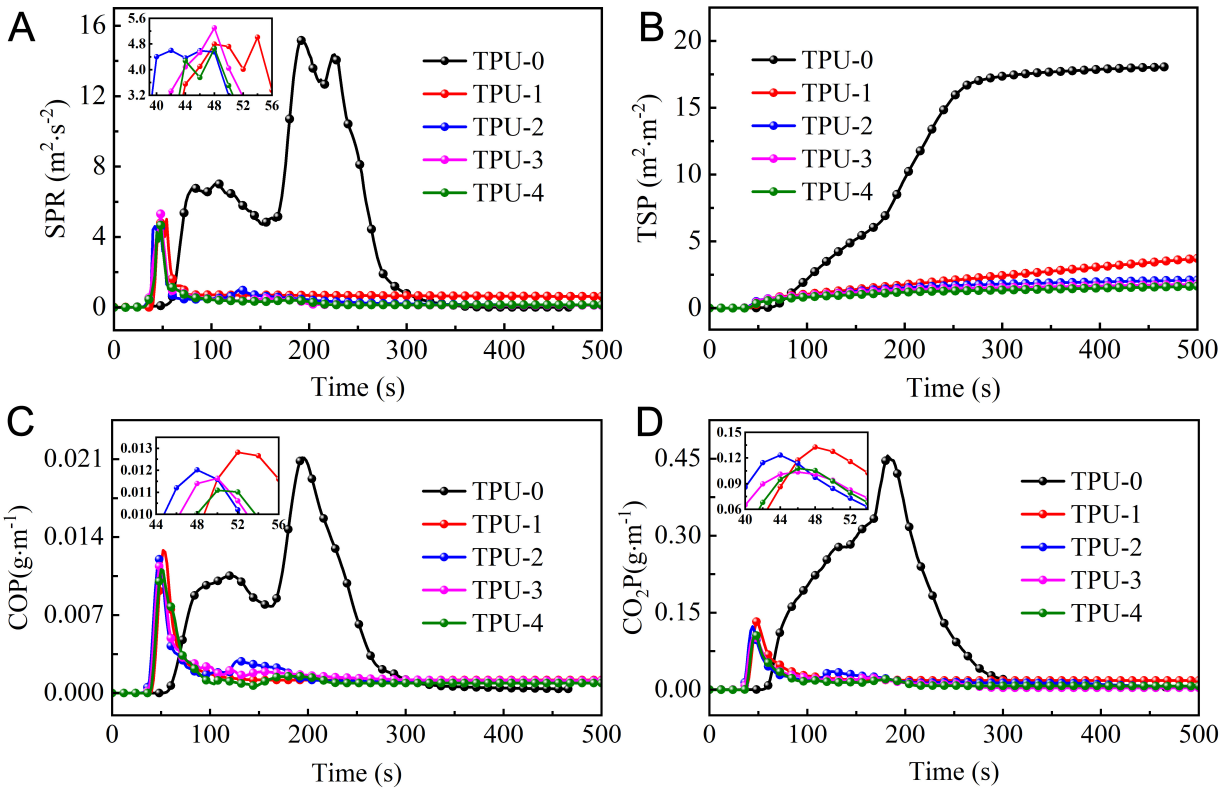

Figure 7. Release profiles of key fire effluents from TPU and its composites: (A) SPR, (B) TSP, (C) CO, and (D) CO_2 generation. TPU: Thermoplastic polyurethane; SPR: smoke production rate; TSP: total smoke production.

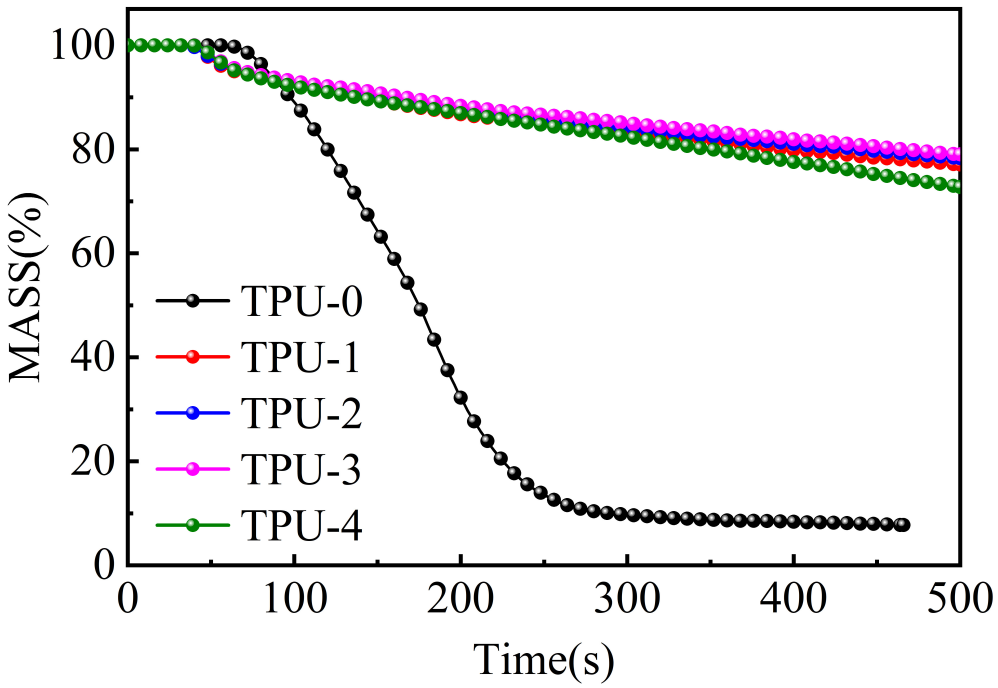

Figure 8. MASS curves of the composites during the cone test. TPU: Thermoplastic polyurethane; MASS: mass loss rate.

Figure 10 further presents the characterization of the char layer composition via Raman spectroscopy. The D and G bands, defining features of the carbon structure, are resolved at 1,360 and 1,590 cm^{-1} in the Raman spectrum. A lower I_D/I_G value serves as a reliable proxy for enhanced structural ordering within the carbon

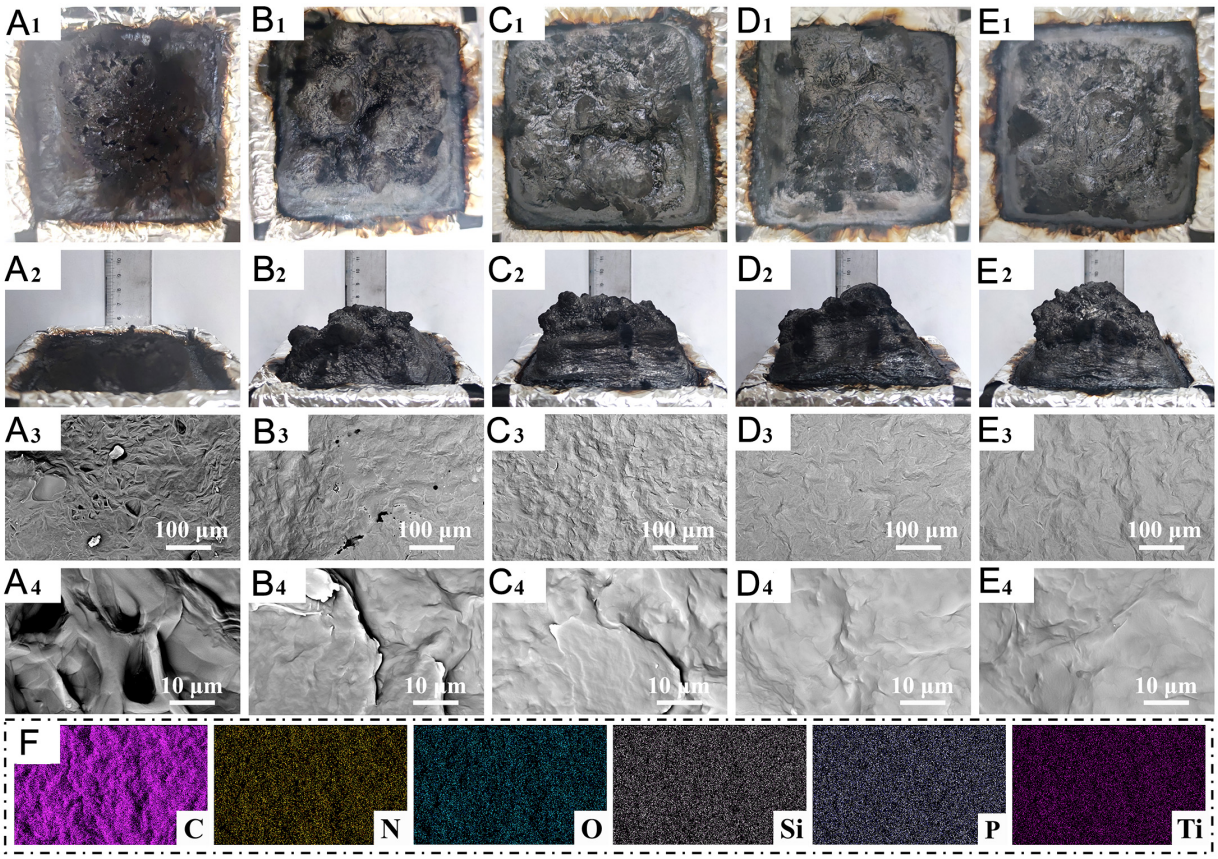

Figure 9. Morphological Evolution and Elemental Architecture of Post-Combustion Residues. (A-E) Digital and scanning electron micrographs of chars from: (A) Neat TPU, and composites incorporating (B) APP, (C) APP-1BL, (D) APP-2BL, (E) APP-3BL' (F) Corresponding spatial element distribution for the TPU/APP@PEI@SiO_2@MXene-3BL composite. APP: Ammonium polyphosphate; TPU: thermoplastic polyurethane; PEI: polyethyleneimine.

lattice, which implies a more compact carbon layer[44,45]. Pure TPU yields the highest disorder index, I_D/I_G = 2.14. Incorporating the flame retardants lowers this ratio markedly for the TPU composites, reflecting a more graphitized char, and TPU/APP@PEI@SiO_2@MXene exhibits a lower I_D/I_G value compared to TPU/APP. In addition, as the number of PEI@SiO_2@MXene layers rises, TPU/APP@PEI@SiO_2@MXene displays a trend of decreasing I_D/I_G values, which suggests that the TPU/APP-3L composite exhibits the highest level of graphitization in its char layer. This is linked to the catalytic action of transition metals within MXene.

Mechanism of flame retardancy in the composites

The surface composition and elemental speciation within the TPU/APP-3BL char residues were interrogated by XPS. As illustrated in Figure 11, the results verified the presence of elements such as Ti, Si, P, N, C, and O. For Ti, the main characteristic peaks correspond to Ti-O, Ti^{2+}, and Ti-C, indicating that the Ti element predominantly exists as TiO_2 compounds. XPS of the char residues resolves the Si 2p region into two components-103.5 eV (SiO_2) and 102.6 eV (Si-O-Si)-confirming the silica architecture generated during combustion. These silicon-based species are conducive to forming a continuous, protective silica film on the char surface. Meanwhile, the P 2p spectrum shows two dominant peaks at 135.1 and 134.1 eV, attributable to P=O and P-O bonds, which originate from the decomposition products of APP. Additionally, the deconvoluted O 1s spectrum exhibits multiple components, including C-O, C=O, Si-O, P-O/P=O, and Ti-O, collectively confirming the successful formation of a silicon-enriched protective layer within the carbon matrix. The high-resolution C 1s spectrum shows four peaks, which correspond to C-O, C-C, C=C, and C-Ti bonds, respectively-clearly indicating that the carbon layer is mainly composed of C-C bonds.

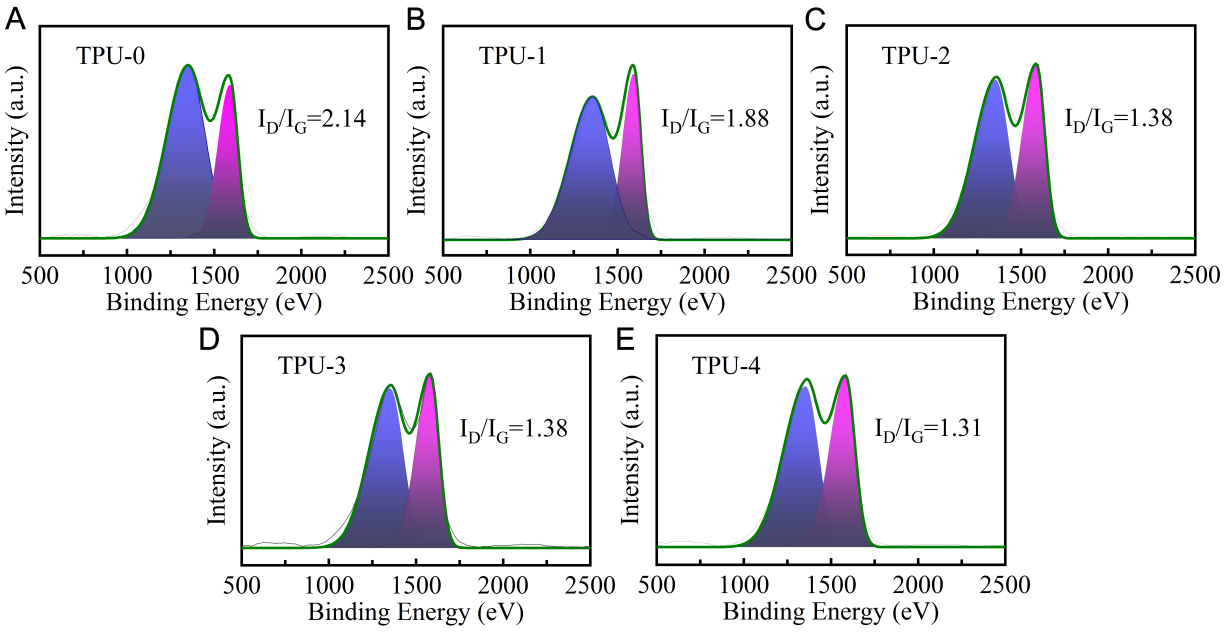

Figure 10. Micro-Raman Analysis of Post-Combustion Carbon Structures. Comparative spectra for pristine TPU and its composite counterparts: (A) Pure TPU, (B) TPU/APP, (C) TPU/APP-1BL, (D) TPU/APP-2BL, (E) TPU/APP-3BL. TPU: Thermoplastic polyurethane; APP: ammonium polyphosphate.

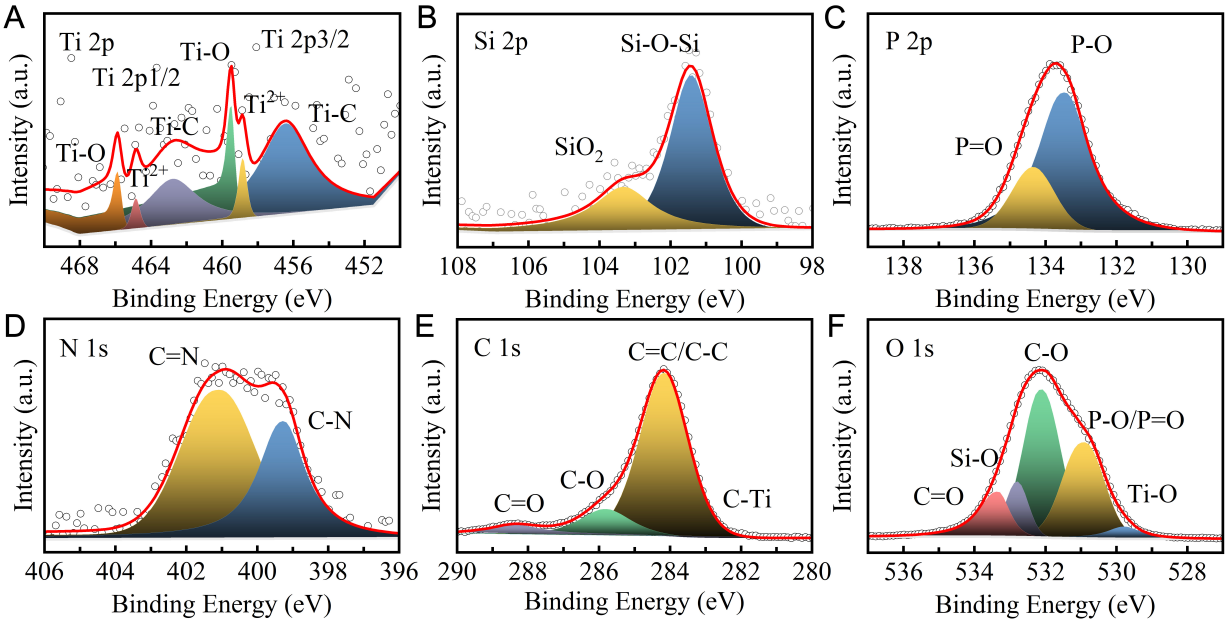

Figure 11. Chemical State Profiling of the Char Surface. High-resolution XPS spectra acquired from the TPU/APP-3BL composite residue: (A) Ti 2p, (B) Si 2p, (C) P 2p, (D) N 1s, (E) C 1s, and (F) O 1s. TPU: Thermoplastic polyurethane; XPS: X-ray photoelectron spectroscopy; APP: ammonium polyphosphate.

To conduct a deeper investigation into the gaseous thermal degradation products, Thermogravimetric-infrared spectroscopy was utilized to detect and analyze TPU and its composite materials. From Figure 12, it is observable that TPU exhibits the highest peak intensity for its thermal degradation products, whereas the TPU/APP-3BL composites show the lowest peak intensity in this regard. Introducing flame retardants notably diminishes the production of gaseous thermal degradation byproducts, which implies that the APP and shell structures impede TPU's thermal degradation processes, thus

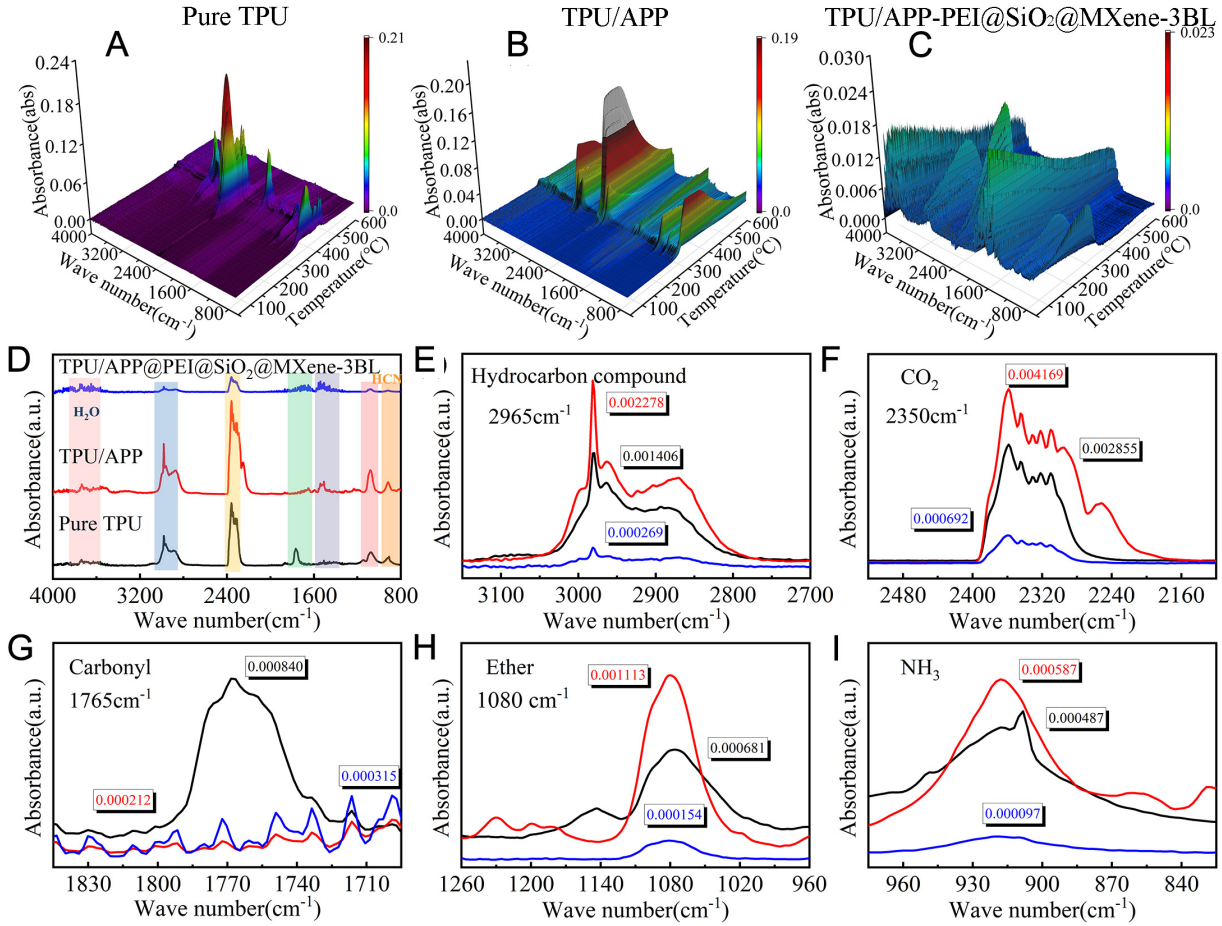

Figure 12. 3D TG-IR spectra of (A) Pure TPU, (B) TPU/APP, and (C) TPU/APP-3BL; the gases products at maximum degradation rate; absorption peak forhydrocarbon compound, carbonyl, aromatic compounds, ethers and Aromatic hydrocarbon (D-I). TPU: Thermoplastic polyurethane; APP: ammonium polyphosphate; PEI: polyethyleneimine; 3D TG-IR: three-dimensional thermogravimetric analysis-infrared spectroscopy.

improving its fire resistance. Moreover, adding flame retardants did not change the types of thermal degradation products throughout TPU's thermal degradation procedure. All three TPU systems released analogous volatiles: 3,600-3,900 cm^{-1} (H_2O), 2,980 cm^{-1} (hydrocarbons), 2,360 cm^{-1} (CO_2), 1,770 cm^{-1} (carbonyls), 1,540-1,420 cm^{-1} (aromatics), 1,080 cm^{-1} (ethers) and 910 cm^{-1} (NH_3)[46-48]. Relative to neat TPU, the TPU/APP-3BL composite shows a pronounced drop in the mass spectral signatures of key gas-phase pyrolyzates-specifically aliphatic/aromatic hydrocarbons, carbonyl-containing moieties, and oxygenated volatiles, which constitutes direct evidence that the composite system favors a solid-phase carbonization pathway over gaseous fuel production when exposed to thermal stress. Additionally, the peak intensity corresponding to CO_2 release in TPU/APP-3BL composites is the lowest, aligning with the cone calorimeter test results. The spectral band observed at 908 cm^{-1} is ascribed to NH_3 (a non-flammable gas), implying that the APP-3BL shell layer also aids in suppressing toxic gas emission.

These observations allow us to advance a consolidated flame-retardant scenario for the TPU composites, sketched in Figure 13. This enhanced performance arises from the synergy among phosphorus, nitrogen, metal, silica, and layered structures, which can be specifically divided into the following: (1) Upon heating, APP releases potent acids that dehydrate the polymer, fostering catalytic charring and leaving an insulating carbon barrier over the substrate; (2) APP, acting concurrently as an acid precursor and a gas-yielding compound, engages in a char-swelling fire suppression mechanism in TPU. This interaction yields a highly

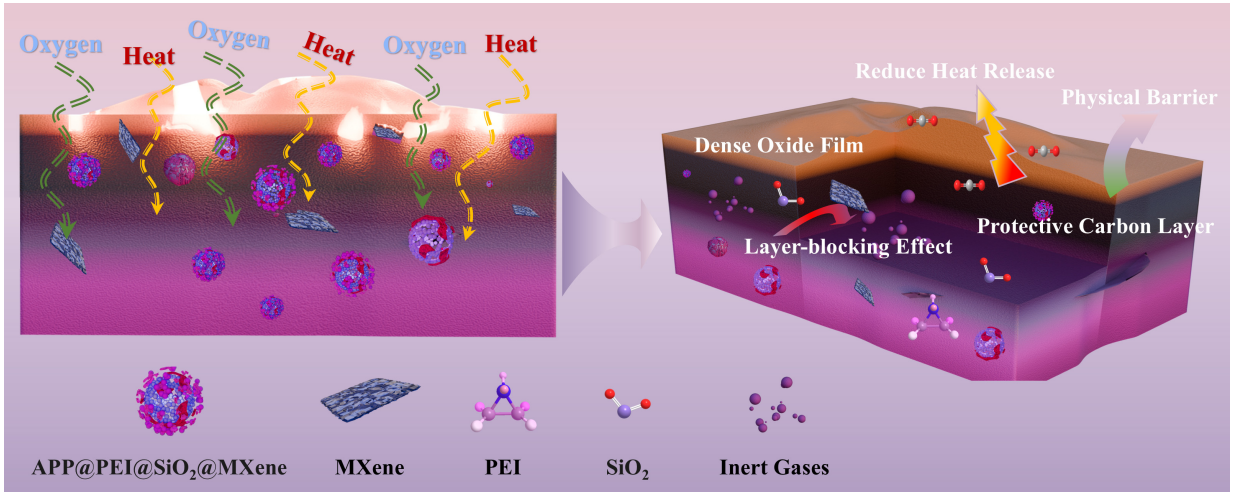

Figure 13. Probable mechanism of flame retardancy for TPU/APP-3BL composites. TPU: Thermoplastic polyurethane; APP: ammonium polyphosphate; PEI: polyethyleneimine.

inflated cohesive char crust, effectively obstructing the transfer of heat and oxygen, lengthening the effusion pathway for flammable volatiles, and curtailing the release of combustible smokes and enthalpy[49,50]; (3) NH_3 generated from APP decomposition dilutes combustible gases and oxygen, while MXene nanosheets block gas transmission. The two synergistically inhibit combustible gas diffusion and enhance gas-phase flame retardancy; (4) After being heated, the silicon-based flame retardant generates a dense SiO_2 oxide film on the matrix's surface, thus reinforcing the char layer; (5) When APP decomposes together with PEI and TPU, it yields inert gases including N_2, H_2O, and NH_3, thereby diluting the oxygen and combustible gases. To sum up, Compared with thermally unstable metal-organic frameworks (MOFs) and graphene oxide prone to agglomeration, the SiO_2/MXene composite shell, by virtue of its synergistic effect, enhances char layer compactness, improves smoke suppression efficiency, achieves gas-solid phase synergistic flame retardancy, significantly optimizes the flame retardant efficiency of APP, and is compatible with TPU while enhancing flame retardant performance.

CONCLUSIONS

To elevate the fire-inhibiting performance of APP, MXene and SiO_2 are utilized as shell materials, enabling the preparation of nano-material encapsulated APP via a sequential assembly approach, and Synergistic flame-retardant action boosts the fire-proofing efficiency of TPU. As for the TPU/APP@PEI@SiO_2@MXene composites, the TPU composites have improved interfacial cohesiveness and dispersion. The TPU composites are endowed with better thermostability, fire resistance, and smoke suppression properties simultaneously. Thermal stability analysis shows that the coated APP remarkably enhances the composite's thermal resistance, as verified by cone calorimeter tests: compared to unmodified TPU, the coated APP endows the material with improved fire safety, reducing pHRR by 71.96% and THR by 79.0%. It also exhibits excellent smoke suppression, with significant declines in the composite's SPR, TSP, YCO, and YCO_2. SEM, TG-IR, XPS, and Raman characterizations confirm that APP@PEI@SiO_2@MXene forms a denser, more graphitic char layer, whose shielding effect effectively inhibits the emission of volatile pyrolysis products. This system can fully combine the action mechanism of SiO_2 and MXene in both the condensed phases and can achieve outstanding flame-retardant efficiency with lower content.

DECLARATIONS

Authors' contributions

Conceptualization: Qian, X.;
Investigation: Qian, X.; Shi, C.

Methodology: Qian, X. Shi, C.; Pan, Y. T.
Formal analysis: Wan, M.
Writing-original draft: Qian, X.; Wan, M.; Chen, L.
Supervision: Hou, Y.; Shi, C.; Che, H.; Jing, J.; Pan, Y. T.
Writing-review & editing: Wan, M.; Li, J.
Funding acquisition: Qian, X.; Shi, C.; Wan, M.; Li, J.
All authors have read and agreed to the published version of the manuscript

Availability of data and materials

The data that support the findings of this study are available from the corresponding author upon reasonable request.

AI and AI-assisted tools statement

During the preparation of this manuscript, the AI tool ChatGPT (version 5.4, released 2026-03-05) was used solely for language polishing and color optimization of the Graphical Abstract. The tool did not influence the study design, data collection, analysis, interpretation, or the scientific content of the work. All authors take full responsibility for the accuracy, integrity, and final content of the manuscript.

Financial support and sponsorship

This work was supported by the National Natural Science Foundation of China (No. 52274232, 52304261, 52504218), Central Fundamental Research Funds of CASS of China (No. 2024JBKY05, 2024JBKY03), Beijing Nova Program (No. 20220484050, 20230484417), Natural Science Foundation of Hebei Province (No. E2025508059), and China Postdoctoral Science Foundation (No. 2025M771796).

Conflicts of interest

All authors declared that there are no conflicts of interest.

Ethical approval and consent to participate

Not applicable.

Consent for publication

Not applicable.

REFERENCES

1. Yin, L.; Zhang, J.; Luo, J.; et al. Janus-inspired alternating architecture CNF/MXene/$ZnFe_2O_4$@PANI composite films with outstanding electromagnetic interference shielding and Joule heating. *J. Mater. Sci. Technol.* **2025**, *223*, 275-86. DOI
2. Xiao, F.; Peng, W.; Li, K.; Yuan, B.; Fontaine, G.; Bourbigot, S. A highly fire-safe wood hybrid based on delignification and multi-component co-impregnation strategies. *Constr. Build. Mater.* **2025**, *489*, 142360. DOI
3. Wang, H.; Wang, Y.; Li, T.; et al. Nature-inspired, heat & noise-insulation, highly robust MOFs-based hybrid fire-retardant coatings with easy-recycling feature. *Adv. Funct. Mater.* **2025**, *35*, 2500800. DOI
4. Ozcelik, G.; Elcin, O.; Guney, S.; Erdem, A.; Hacioglu, F.; Dogan, M. Flame-retardant features of various boron compounds in thermoplastic polyurethane and performance comparison with aluminum trihydroxide and magnesium hydroxide. *Fire. Mater.* **2022**, *46*, 1020-33. DOI
5. Afshari, M.; Dinari, M. Improving the Reaction-to-fire properties of thermoplastic polyurethane by new phosphazene-triazinyl-based covalent organic framework. *ACS. Appl. Mater. Interfaces.* **2022**, *14*, 49003-13. DOI
6. Wang, H. Wang ,Y.; Gao, J.; Zhu, Z.; Xiao, F. Synergistic engineering of phosphaphenanthrene and ionic liquids for unlocking flame retardant multifunctional epoxy resin with high performances. *Polym. Degrad. Stab.* **2025**, *239*, 111407. DOI
7. Han, S.; Yang, F.; Li, Q.; Sui, G.; Kalimuldina, G.; Araby, S. Synergetic effect of α-ZrP nanosheets and nitrogen-based flame retardants on thermoplastic polyurethane. *ACS. Appl. Mater. Interfaces.* **2023**, *15*, 17054-69. DOI PubMed

8. Li, Y.; Li, Y.; Hu, W.; Wang, D. Cobalt ions loaded polydopamine nanospheres to construct ammonium polyphosphate for the improvement of flame retardancy of thermoplastic polyurethane elastomer. *Polym. Degrad. Stab.* **2022**, *202*, 110035. DOI
9. Shi, Y.; Yao, A.; Han, J.; et al. Architecting fire safe hierarchical polymer nanocomposite films with excellent electromagnetic interference shielding via interface engineering. *J. Colloid. Interface. Sci.* **2023**, *640*, 179-91. DOI PubMed
10. Bourbigot, S.; Turf, T.; Bellayer, S.; Duquesne, S. Polyhedral oligomeric silsesquioxane as flame retardant for thermoplastic polyurethane. *Polym. Degrad. Stab.* **2009**, *94*, 1230-7. DOI
11. Cai, W.; Zhan, J.; Feng, X.; et al. Facile construction of flame-retardant-wrapped molybdenum disulfide nanosheets for properties enhancement of thermoplastic polyurethane. *Ind. Eng. Chem. Res.* **2017**, *56*, 7229-38. DOI
12. Patrick Lim, W.; Mariatti, M.; Chow, W.; Mar, K. Effect of intumescent ammonium polyphosphate (APP) and melamine cyanurate (MC) on the properties of epoxy/glass fiber composites. *Compos. Part. B. Eng.* **2012**, *43*, 124-8. DOI
13. Matykiewicz, D.; Przybyszewski, B.; Stanik, R.; Czulak, A. Modification of glass reinforced epoxy composites by ammonium polyphosphate (APP) and melamine polyphosphate (PNA) during the resin powder molding process. *Compos. Part. B. Eng.* **2017**, *108*, 224-31. DOI
14. Zhao, C.; Liu, Y.; Wang, D.; Wang, D.; Wang, Y. Synergistic effect of ammonium polyphosphate and layered double hydroxide on flame retardant properties of poly(vinyl alcohol). *Polym. Degrad. Stab.* **2008**, *93*, 1323-31. DOI
15. Shao, Z.; Deng, C.; Tan, Y.; Chen, M.; Chen, L.; Wang, Y. Flame retardation of polypropylene via a novel intumescent flame retardant: Ethylenediamine-modified ammonium polyphosphate. *Polym. Degrad. Stab.* **2014**, *106*, 88-96. DOI
16. Guan, Y.; Huang, J.; Yang, J.; Shao, Z.; Wang, Y. An effective way to flame-retard biocomposite with ethanolamine modified ammonium polyphosphate and its flame retardant mechanisms. *Ind. Eng. Chem. Res.* **2015**, *54*, 3524-31. DOI
17. Wu, C.; Wang, X.; Zhang, J.; Cheng, J.; Shi, L. Microencapsulation and surface functionalization of ammonium polyphosphate via in-situ polymerization and thiol-ene photograted reaction for application in flame-retardant natural rubber. *Ind. Eng. Chem. Res.* **2019**, *58*, 17346-58. DOI
18. Wang, B.; Qian, X.; Shi, Y.; et al. Cyclodextrin microencapsulated ammonium polyphosphate: preparation and its performance on the thermal, flame retardancy and mechanical properties of ethylene vinyl acetate copolymer. *Compos. Part. B. Eng.* **2015**, *69*, 22-30. DOI
19. Xu, Y.; Yan, C.; Du, C.; et al. High-strength, thermal-insulating, fire-safe bio-based organic lightweight aerogel based on 3D network construction of natural tubular fibers. *Compos. Part. B. Eng.* **2023**, *261*, 110809. DOI
20. Zhu, Z.; Deng, X.; Ye, Y.; et al. Hierarchical cyclic phosphates@MIL-101 toward improving thermal stability, fire retardancy, UV shielding, and mechanical performance of thermoplastic polyurethane based on nanoconfinement engineering. *Colloids. Surf. A. Physicochem. Eng. Asp.* **2026**, *731*, 139112. DOI
21. Shi, Y.; Wu, S.; Chen, J.; et al. Hierarchically building flame retardant and flexible electromagnetic interference shielding composites with tunable mechanism. *J. Mater. Sci. Technol.* **2025**, *239*, 39-54. DOI
22. Xiao, F.; He, W.; Shao, W.; et al. Natural tannic acid-based intumescent coating towards efficient fire resistance and thermal performance for steel structure. *Int. J. Biol. Macromol.* **2025**, *322*, 146983. DOI PubMed
23. Xu, Y.; Hu, H.; Tao, B.; Yin, R.; Liu, L.; Li, B. Safe and economical preparation of amino acid-derived bio-based triazine char-forming agent for efficient intumescent flame retardant polypropylene. *Constr. Build. Mater.* **2025**, *484*, 141876. DOI
24. Xiao, F.; Huo, X.; Shao, W.; Yuan, B.; Li, K.; Zhu, L. A versatile eco-friendly intumescent coating imparts excellent fire protective performance for steel structures and batteries. *Prog. Org. Coat.* **2026**, *212*, 109850. DOI
25. Zhang, W.; Wang, H.; Ji, S.; et al. Mechanically durable and flame retardant CNF/PPy-MXene aerogel composites toward superior electromagnetic shielding with ultra-low reflectivity. *Colloids. Surf. A. Physicochem. Eng. Asp.* **2025**, *723*, 137294. DOI
26. Ding, H.; Wang, J.; Wang, C.; et al. Intermolecular hydrogen bonding enabling mechanically robust, thermally stable, and solvent-resistance bio-based polyimine networks. *Compos. Part. A. Appl. Sci. Manuf.* **2025**, *196*, 109006. DOI
27. Lian, R.; Gao, Q.; Zhao, Z.; et al. Hierarchical MXene@PBA nanohybrids towards high-efficiency flame retardancy and smoke suppression of robust yet tough polymer nanocomposites at ultra-low additions. *Compos. Part. B. Eng.* **2023**, *267*, 111074. DOI
28. Ding, H.; Liu, L.; Wang, C.; et al. Highly transparent, mechanically strong, recyclable, and flame-retardant vanillin-modified poly(urethane-urea) elastomers via dynamic oxime-urethane bonds and hydrogen bonds. *Chem. Eng. J.* **2025**, *514*, 163416. DOI
29. Luo, J.; Zhou, K.; Ding, Y.; Yin, L.; Hou, Y. Dual self-antiaggregating hybrid nanoarchitectonics for synergistic effects on the fire safety of intumescent flame retardant epoxy resins. *Adv. Powder. Technol.* **2025**, *36*, 104815. DOI
30. Lin, B.; Yuen, A. C. Y.; Chen, T. B. Y.; et al. Experimental and numerical perspective on the fire performance of MXene/Chitosan/Phytic acid coated flexible polyurethane foam. *Sci. Rep.* **2021**, *11*, 4684. DOI PubMed PMC
31. Wang, J.; Ding, H.; Bi, Z.; et al. “Rigid-Flexible” structured polyimine/graphite felt composites with excellent fire Resistance, electromagnetic shielding and recyclability. *Chem. Eng. J.* **2024**, *501*, 157610. DOI
32. Yin, L.; Zhou, M.; Shi, Y.; Zhou, K. Construction of superhydrophobic flexible polyurethane with dual nano-enhancement effect for solar-assisted high-viscosity oil cleanup and oil-water separation. *Appl. Surf. Sci.* **2024**, *660*, 159971. DOI

33. Zhang, L.; Huang, Y.; Dong, H.; Xu, R.; Jiang, S. Flame-retardant shape memory polyurethane/MXene paper and the application for early fire alarm sensor. *Compos. Part. B. Eng.* **2021**, *223*, 109149. DOI
34. Liu, C.; Wu, W.; Shi, Y.; et al. Creating MXene/reduced graphene oxide hybrid towards highly fire safe thermoplastic polyurethane nanocomposites. *Compos. Part. B. Eng.* **2020**, *203*, 108486. DOI
35. Kandola, B.; Pornwannachai, W.; Ebdon, J. Flame retardance of a bio-based furan resin: effects of added flame retardants. *Polym. Degrad. Stab.* **2024**, *220*, 110637. DOI
36. Geschwindner, C.; Goedderz, D.; Li, T.; Bender, J.; Böhm, B.; Dreizler, A. The effects of various flame retardants on the combustion of polypropylene: combining optical diagnostics and pyrolysis fragment analysis. *Polym. Degrad. Stab.* **2023**, *211*, 110321. DOI
37. Tian, F.; Mao, W.; Xu, X. Effect of a layered combination of APP and TBC on the mechanics and flame retardancy of poplar strandboards. *Constr. Build. Mater.* **2023**, *401*, 132881. DOI
38. Ramachandran, R.; Rajavel, K.; Xuan, W.; Lin, D.; Wang, F. Influence of $Ti_3C_2T_x$ (MXene) intercalation pseudocapacitance on electrochemical performance of Co-MOF binder-free electrode. *Ceram. Int.* **2018**, *44*, 14425-31. DOI
39. Jiao, E.; Wu, K.; Liu, Y.; et al. Ultrarobust MXene-based laminated paper with excellent thermal conductivity and flame retardancy. *Compos. Part. A. Appl. Sci. Manuf.* **2021**, *146*, 106417. DOI
40. Jia, Z.; Li, Z.; Ma, S.; et al. Constructing conductive titanium carbide nanosheet (MXene) network on polyurethane/polyacrylonitrile fibre framework for flexible strain sensor. *J. Colloid. Interface. Sci.* **2021**, *584*, 1-10. DOI PubMed
41. Chen, W.; Wang, L.; Liu, G. Synthesis of ammonium polyphosphate with crystalline form V (APP-V) from melamine polyphosphate (MPP). *Polym. Degrad. Stab.* **2012**, *97*, 2567-70. DOI
42. Wang, D.; Zhang, D.; Yang, Y.; Mi, Q.; Zhang, J.; Yu, L. Multifunctional latex/polytetrafluoroethylene-based triboelectric nanogenerator for self-powered organ-like MXene/metal-organic framework-derived CuO nanohybrid ammonia sensor. *ACS. Nano.* **2021**, *15*, 2911-9. DOI
43. Zhao, W.; Lei, Y.; Zhu, Y.; et al. Hierarchically structured Ti_3C_2T MXene paper for Li-S batteries with high volumetric capacity. *Nano. Energy.* **2021**, *86*, 106120. DOI
44. Ali, W.; Zilke, O.; Danielsiek, D.; et al. Flame-retardant finishing of cotton fabrics using DOPO functionalized alkoxy- and amido alkoxysilane. *Cellulose* **2023**, *30*, 2627-52. DOI
45. Ye, X.; Feng, Y.; Tian, P.; et al. Engineering two nitrogen-containing polyhedral oligomeric silsesquioxanes (N-POSSs) to enhance the fire safety of epoxy resin endowed with superior thermal stability. *Polym. Degrad. Stab.* **2022**, *200*, 109946. DOI
46. Lu, W.; Jin, Z. Synthesis of phosphorus/nitrogen containing intumescent flame retardants from p-hydroxybenzaldehyde, vanillin and syringaldehyde for rigid polyurethane foams. *Polym. Degrad. Stab.* **2022**, *195*, 109768. DOI
47. Battig, A.; Markwart, J. C.; Wurm, F. R.; Schartel, B. Hyperbranched phosphorus flame retardants: multifunctional additives for epoxy resins. *Polym. Chem.* **2019**, *10*, 4346-58. DOI
48. Xu, F.; Zhang, G.; Wang, P.; Dai, F. Durable and high-efficiency casein-derived phosphorus-nitrogen-rich flame retardants for cotton fabrics. *Cellulose* **2022**, *29*, 2681-97. DOI
49. Zhai, R.; Yang, Z.; Chen, Y.; Zhang, Y.; Lv, Z. Design novel environmentally-friendly flame retardants. *Combust. Sci. Technol.* **2022**, *195*, 2474-90. DOI
50. Yi, C.; Xu, C.; Sun, N.; et al. Flame-retardant and transparent poly(methyl methacrylate) composites based on phosphorus-nitrogen flame retardants. *ACS. Appl. Polym. Mater.* **2022**, *5*, 846-55. DOI